

## Evaporative Refrigeration Effect in Evaporation and Condensation between Two Parallel Plates

Peiyi Chen,<sup>1, a)</sup> Qin Li,<sup>1, b)</sup> and Gang Chen<sup>2, c)</sup>

<sup>1)</sup>*Department of Mathematics, University of Wisconsin-Madison, Madison, WI 53706*

<sup>2)</sup>*Department of Mechanical Engineering, Massachusetts Institute of Technology, Cambridge, MA 02139*

(Dated: April 15, 2025)

It is well-known that evaporation can lead to cooling. However, little is known that evaporation can actually create a refrigeration effect, i.e., the vapor phase temperature can drop below the temperature of the liquid-vapor interface. This possibility was recently pointed out via modeling based on a quasi-continuum approach. Experimental evidence for this effect has been scarce so far. Here, we examine evaporation and condensation between two parallel plates, including the liquid films on both sides, by coupling the solution of the Boltzmann transport equation in the vapor phase with the continuum treatments in both liquid films. Our solution shows that the vapor phase temperature at the evaporating side can be much lower than the coldest wall temperature at the condensing surface, i.e., the evaporative refrigeration effect. Our work not only re-affirms the refrigeration effect, but clarifies that this effect is caused by two mechanisms. At the interface, the asymmetry in the distribution between the outgoing and the incoming molecules creates a cooling effect, which is the dominant mechanism. Additional cooling occurs within the Knudsen layer due to the sudden expansion similar to the Joule-Thomson effect, although with subtle differences in that the interfacial expansion is not an isenthalpic process. Our work will motivate future experiments to further confirm this prediction and explore its potential applications in air-conditioning and refrigeration.

---

<sup>a)</sup>Electronic mail: pchen345@wisc.edu.

<sup>b)</sup>Electronic mail: qinli@math.wisc.edu.

<sup>c)</sup>Electronic mail: gchen2@mit.edu.

## I. INTRODUCTION

In the Joule-Thomson effect, the sudden expansion of a fluid can lead to the fluid temperature at the outlet dropping below that at the inlet, which is the underlying principle for most air-conditioning and refrigeration systems. Evaporation of a fluid can also lead to cooling, i.e., the evaporative cooling, which is used in some air-conditioning systems<sup>1,2</sup>. Putting a cup of water in air, evaporation cools down the liquid and the surrounding air. In this case, temperature of the surrounding is higher than liquid and heat is transferred from the surrounding to water, i.e., the temperature is inverted. Despite its familiarity, the unconventional temperature distribution can cause confusion: evaporation seems to carry heat away from the liquid while surrounding air transfers heat to the liquid. Although this superficial contradiction to the second law of thermodynamics – heat always spontaneously flows from hot to cold regions – can be easily resolved by realizing that evaporation is driven by the chemical potential difference between liquid water and water vapor in air, it does exemplify the complexity with evaporation. In this work, we discuss another little known consequence of evaporation: the evaporating vapor can cool below the liquid temperature, i.e., the evaporative refrigeration effect.

The evaporative refrigeration effect is related to temperature and density discontinuities at an evaporating interface. Such discontinuities were anticipated by pioneering work of Hertz, Knudsen, and Schrage<sup>3–6</sup>. In 1971, Pao<sup>7</sup> predicted the existence of these discontinuities at an evaporating surface, starting from the Boltzmann transport equation. In the same year, he also investigated the parallel plate problem: evaporation from one surface and condensation on the other<sup>8</sup>. Pao predicted that the vapor phase temperature profile is inverted: lower at the evaporation side and higher at the condensation side, opposing to the applied temperature difference between the hot evaporating wall and the cold condensing wall. Pao did not include any liquid film on either the evaporating or the condensing side. Instead, he simply specified that the walls are at the saturation conditions. Many subsequent studies have used the same assumptions to investigate both the single interface evaporation and the two parallel plate problems based on solving the Boltzmann transport equation numerically<sup>9–15</sup>, or via taking its moments<sup>16–18</sup>, Monte Carlo simulations<sup>19</sup>, and molecular dynamics simulations<sup>20–29</sup>. Asymptotic solutions and discontinuous boundary conditions have also been derived<sup>30–34</sup> and used to couple to continuum treatment<sup>35,36</sup>. None of these

studies, however, have discussed possible refrigeration effect in the evaporation process.

Experimental measurements of the interfacial temperature discontinuities had also been reported, pioneered by Ward and co-workers<sup>37-51</sup>, as well-summarized by Jafari et al.<sup>52</sup>. Most of these experiments reported that the vapor side has a higher temperature than that of the liquid surface, although a few experiments reported that the vapor side could actually be at a lower temperature than that of the liquid interface<sup>46,47,50</sup>. These experiments cannot be modeled by directly solving the Boltzmann transport equation since the dimensions of the experiments are much larger than the vapor mean free path. Besides, previous effort in solving the Boltzmann transport equation had completely neglected the liquid layer. Approximate boundary conditions such as the Hertz-Knudsen and the Schrage equations<sup>5,6</sup> have too many variables that cannot be uniquely used to determine the interfacial temperature discontinuities. Such difficulties have motivated alternative modeling approaches<sup>53,54</sup>. None of them predicted a lower temperature at the vapor side.

Chen recently tackled the above difficulties by introducing an additional heat flux condition in addition to the often-used Schrage equation for the mass flux, such that the transport across the Knudsen layer can be approximated by density and temperature discontinuities<sup>55,56</sup>. With these boundary conditions, temperature distributions for both the liquid and vapor sides and temperature and density discontinuities at the interface can be obtained using continuum approximations for both the liquid and the vapor regions. Chen applied such quasi-continuum approach to treat evaporation from and condensation into a single liquid layer and showed that the experimental results in the past can be explained. The vapor side temperature can be lower or higher than that of the liquid surface temperature, depending on the film thickness and the vapor side boundary conditions. The same approach was extended to treat the effect when noncondensable gas is present<sup>57</sup>. For the two parallel plate problem, his model<sup>58</sup> showed temperature inversion as original predicted by Pao<sup>8</sup>. Even more interestingly, the modeling result shows that the vapor region could be significantly colder than the condensing surface temperature: an evaporative refrigeration effect. Such evaporative refrigeration effect may lead to new air-conditioning and refrigeration technologies, which is especially important considering current air-conditioning and refrigeration systems rely heavily on the Joule-Thomson effect, which require compressors and employ refrigerants that are harmful to the environment. These predictions, however, are based on approximative interfacial conditions that neglect the transport within the Knudsen

layer, and hence call for further validation. Most experimental results on evaporation so far showed that the vapor side temperature is higher than that of the liquid surface. The few existing experiments suggesting the vapor side temperature could be lower is within less than  $1^\circ\text{C}$  in the vapor side compared to the liquid interface<sup>46,47,50</sup>.

In this work, we explore the evaporation and condensation problem between two parallel plates including liquid films on both sides, by coupling the Boltzmann transport equation description for the vapor phase to the continuum treatment for the liquid films. Interfacial molecular absorption, reflection, and evaporation are included via the boundary conditions coupling the liquid and the vapor regions. Energy balance is applied at the interface to self-consistently determine the interfacial temperatures of the liquid films and the vapor. Our work confirms the evaporative refrigeration effect. The degree of cooling depends on several key parameters, including the Knudsen number, the liquid film thickness, the vapor-gap thickness, and the accommodation coefficient. Our prediction should stimulate further experiments to validate this evaporative refrigeration effect.

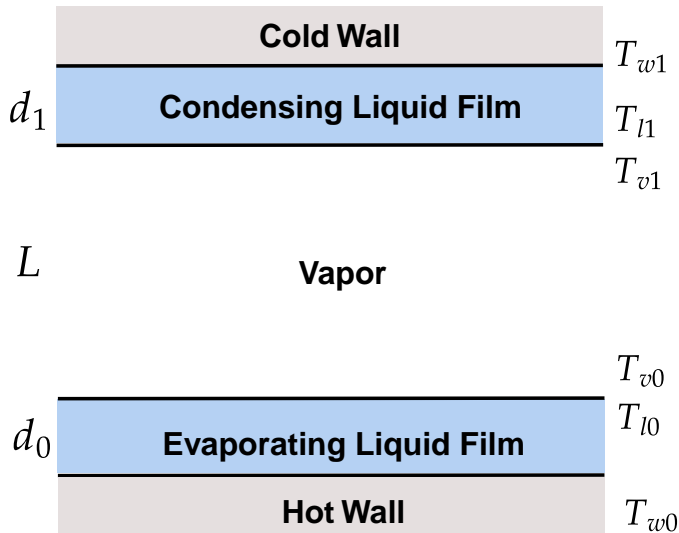


Figure 1: Parallel plate experiment set-up. Here  $d_{0,1}$  are the thicknesses of liquid films,  $L$  represents the thickness of vapor gap.  $T$  denotes the temperature at different locations:  $T_{w0}, T_{w1}$  are the imposed wall temperatures,  $T_{l0}, T_{l1}$  and  $T_{v0}, T_{v1}$  stand for liquid and vapor temperatures at the liquid-vapor interfaces respectively.

## II. RESULTS

We numerically simulate the two parallel plate problem shown in Fig. 1 by solving the Fourier heat equation in the liquid films and the Boltzmann transport equation under the Bhatnagar-Gross-Krook (BGK) approximation in the vapor region<sup>59</sup>. The liquid and the vapor regions are coupled properly at the interfaces, considering the molecular emission, reflection, and condensation. Details of the equations and interfacial conditions are presented in the Method Section. We will focus below discussing the results.

Fig. 2a gives one example clearly showing the evaporative refrigeration effect. The specified wall temperature on the evaporation side is  $T_{w0} = 314\text{K}$  and the condensation side is  $T_{w1} = 304\text{K}$ . We notice that the predicted temperature distribution in the vapor region is inverted: hotter at the condensation side than the evaporation side, consistent with the predictions made by Pao<sup>8</sup> and confirmed by others. Importantly, the vapor temperature in most of the gap region is below the condensing wall temperature, as low as  $299.15\text{K}$ ,  $5\text{K}$  lower than the cold side temperature. This is clearly a refrigeration effect. Large temperature discontinuities exist at the interface. Fig. 2b also plots the interfacial saturation vapor density, which differs from the vapor side density at the interface, i.e., vapor density discontinuities exist.

Chen<sup>56</sup> discussed the origin of the refrigeration effect as arising from the difference in the carrier distribution function at the interfacial region and the continuum region. At the interfacial region, vapor enthalpy in the forward direction is  $2RT$ , where  $R$  is the universal gas constant. While outside the Knudsen layer, the vapor enthalpy is  $2.5RT$ , i.e., the constant pressure specific heat of a monatomic gas. The  $2RT$  is also consistent with thermionic emission<sup>60</sup>, confirm the similarities between electron and molecular emission<sup>55</sup>. However, because Chen's treatment neglected the thickness of the Knudsen layer, he could not pinpoint exactly where cooling happens.

In Fig. 2c, we show the molecular distribution function at the interface. The forward half ( $v_1 > 0$ ), representing the molecules leaving the surface, is clearly different from the incoming half ( $v_1 < 0$ ). The forward enthalpy is  $2RT$  while the distribution incoming to the interface is closer to the diffusion distribution outside the Knudsen layer. This asymmetry in the distribution function creates a large interfacial temperature drop, as is clear in Fig. 2a. This mismatch in the forward going flux and the backward going flux is the main mechanism

for the drop of the vapor phase temperature below that of the liquid interface temperature, and it is the main contributor to the interfacial evaporative refrigeration effect.

Furthermore, Fig. 2a also shows that the vapor temperature drops slightly in the Knudsen layer. To understand the origin of this additional temperature drop, we show in Fig. 2d the total energy flux, the enthalpy flux, and the internal energy flux. We note that the total energy flux is a constant, as expected. The total energy flux can be expressed as the sum of three parts: (1) the heat flux, (2) the enthalpy flux, and (3) the kinetic energy flux. The enthalpy flux can be further decomposed into the sum of the internal energy flux and the pressure work flux. Microscopic expressions for each of these fluxes are given in the Method Section. In the Knudsen layer near the evaporation side, we see that the enthalpy flux increases while the internal energy flux decreases away from the interface. The difference of the two gives the pressure work flux, shown in Fig. 2e, which increases away from the interface. The decreasing internal energy flux leads to additional lower temperature of the vapor phase, i.e., the additional cooling effect. This effect bears similarities to the Joule-Thomson effect in a throttle valve. However, the Joule-Thomson expansion is an isenthalpic process, while the expansion across the Knudsen layer in the evaporation side is not isenthalpic. In fact, the decreasing temperature also leads to decreasing heat flux away from the interface, i.e., more heat conducts into the Knudsen region than conducting out of the region, which partially diminishes the internal energy flux reduction and hence the additional cooling effect across the Knudsen layer, as shown in Fig. 2f. However, under proper conditions, the additional cooling happens.

In Fig. 3, we present effects of different key parameters that impact the refrigeration effect, including the temperature distributions in the gap, the minimum temperature of the vapor achieved and the mass flow rates. For all the conditions, the temperature distributions are inverted. This is not surprising since the previous studies already showed that temperature inversions occurs when  $\beta = \frac{T}{\rho} \frac{d\rho}{dT} = \frac{\Gamma}{RT_0} - 1 \geq \beta_c$ , where  $\Gamma$  is the latent heat and the critical value  $\beta_c$  is about 3.5<sup>8,12,30,58</sup>. For water,  $\beta = 18$  and hence temperature distribution in between the gap is always inverted. We see that among the three parameters, the Knudsen number and the liquid film thickness have strong effects on the cooling. As the liquid film gets thinner, the minimal vapor temperature drops, as demonstrated in Fig. 3a and Fig. 3d, because in this case, the heat transferred through the liquid layer is higher, leading to larger mass flux. Larger accommodation coefficient values lead to usually lower minimal

## Evaporative Refrigeration

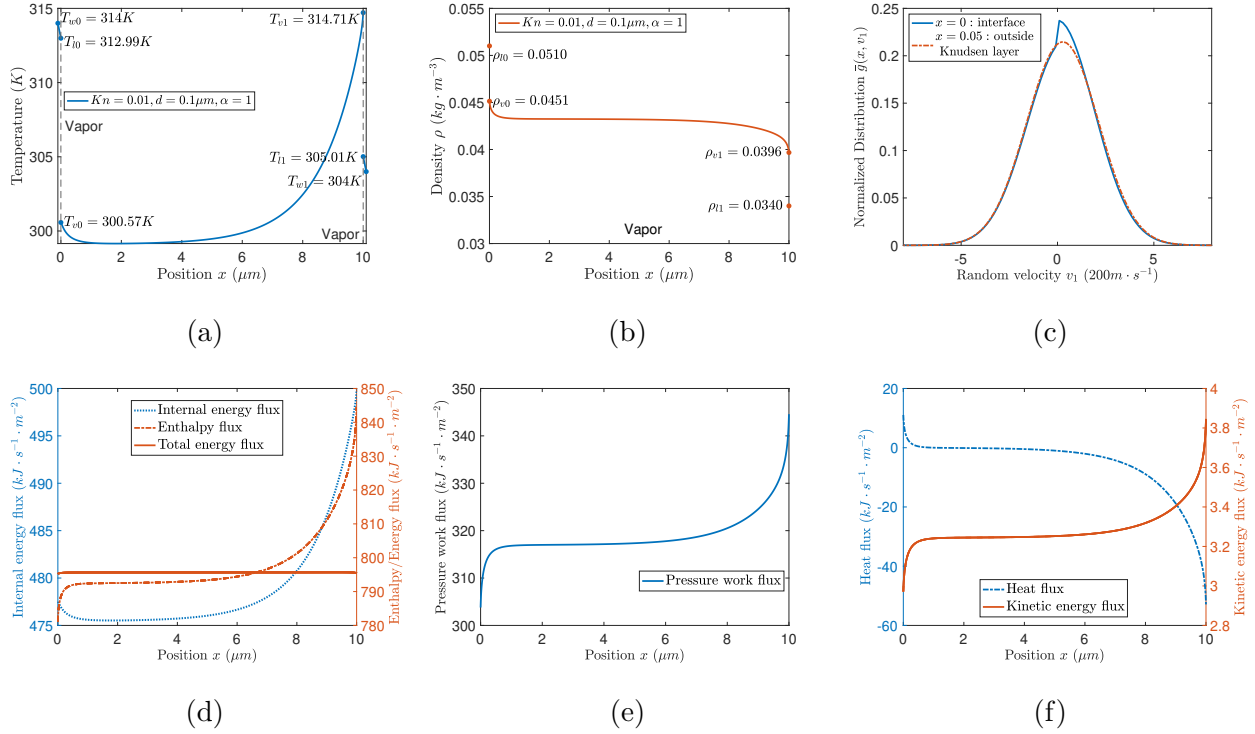


Figure 2: Evaporative refrigeration effect. (a) Temperature distributions showing the evaporative refrigeration effect: the vapor phase temperature at the evaporation side is lower than even the temperature of the cold solid wall, in addition to temperature discontinuities at the interface and inverted vapor phase temperature distribution, (b) density distribution, including the saturation density at the interface, showing the vapor density discontinuity at the interface. Note that density also decreases more rapidly inside the Knudsen layer. (c) Molecular distribution function at the hot liquid-vapor interface and outside the Knudsen layer, showing the cooling happens at the interface due to the difference of the molecular distributions between the molecules leaving and coming towards the interface, (d) distributions of total energy flux, enthalpy flux and internal energy flux, (e) pressure work flux, (f) heat flux and kinetic energy flux. All results for  $(Kn = 0.01, d = 0.1 \mu\text{m}, \alpha = 1)$ .

temperature and larger mass flux [Fig. 3e and Fig. 3f]. Fig. 3b and Fig. 3c show that larger gap, i.e., smaller Knudsen number, leads to lower vapor temperature, i.e., stronger refrigeration effect. This is because at smaller gap size, i.e., larger Knudsen number, more heat reverse conducts back, diminishing the refrigeration effect at the interface.

The results obtained here enable us to compare with results obtained by Chen<sup>58</sup> with the

## Evaporative Refrigeration

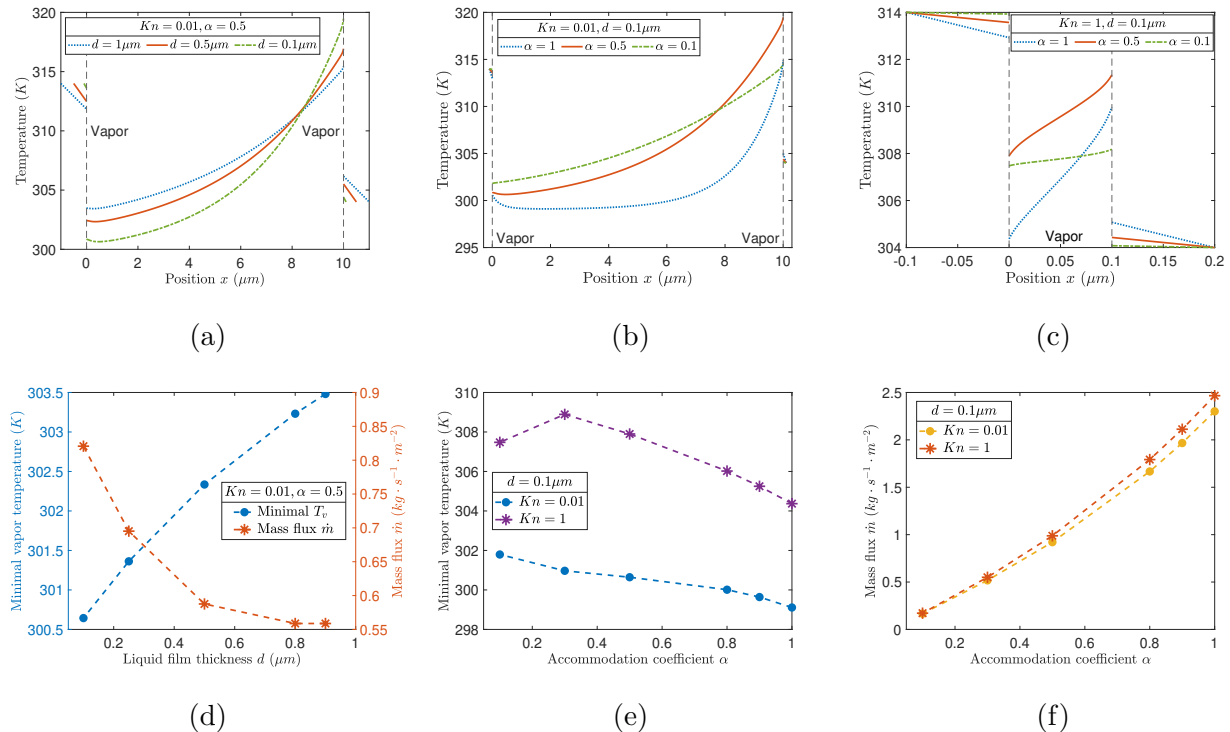


Figure 3: Dependence of Evaporative Refrigeration on Parameters. (a) Effect of liquid film thickness showing thinner liquid film leads to lower vapor temperature, (b) and (c) effect of accommodation coefficient at two different vapor region thicknesses, showing stronger cooling effect with larger accommodation coefficient values and smaller Knudsen numbers (larger vapor gap), (d)-(f) minimal temperature and mass flux at different parameters.

semi-continuum approach through coupling the interfacial mass and heat flux conditions to continuum formulations for both the liquid and the vapor regions, as shown in Fig. 4a and Fig. 4b. The semi-continuum approach predicts similar trends as the solution of the Boltzmann transport equation in terms of the temperature inversion and the discontinuities at the two interfaces. The semi-continuum approaches cannot predict the small temperature reversal inside the Knudsen region that exists in some cases as shown in Fig. 2a. When  $Kn \ll 1$ , the difference between the semi-continuum approach and that of the Boltzmann transport equation is small. However, at larger  $Kn$  numbers (or equivalently, with smaller  $L$ ), the semi-continuum approach gives higher minimum vapor temperature values and thus underestimates the refrigeration effect as shown in Fig. 4c.

To summarize, we verify the existence of the evaporative refrigeration effect through solving the Boltzmann transport equation coupled to liquid films for evaporation and con-

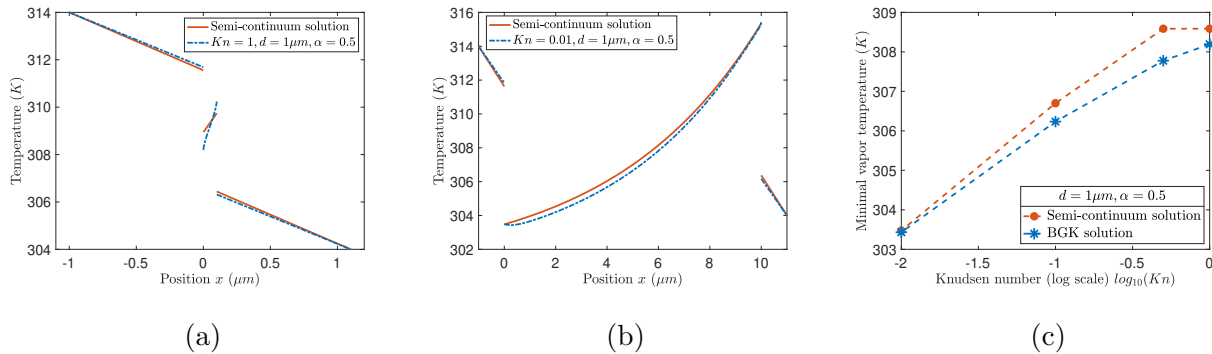


Figure 4: Comparison between semi-continuum solution and BGK solutions. (a) and (b) Temperature distributions at two different Knudsen numbers and (c) minimum vapor temperature vs. Knudsen number (semi-log scale).

condensation between two parallel plates. The vapor phase temperature in the evaporation side can drop below that of the condensing wall. This evaporative refrigeration effect is due mainly to the highly asymmetric molecular distribution function at the liquid-vapor interface, although the continued expansion in the Knudsen layer can lead to additional cooling. Although the inverted temperature profile and temperature discontinuities had been studied before, our treatments include liquid films on both solid walls, making the predictions more realistic. Our rigorous solution shows that the interfacial heat flux and mass flux boundary conditions developed before are appropriate to treat such complicated problems using continuum treats for both the liquid and the vapor phase. Our work should stimulate experimental efforts to validate these predictions and points to directions in experimental validation, since larger gap should be more favorable for experimental observations.

### III. METHOD

The model for the evaporation-condensation phenomenon in this setting is composed of three components: the temperature variation in (hot) liquid film is modeled by the diffusion equation, the vapor phase is modeled by the nonlinear BGK equation, and the temperature variation in (cold) liquid film is once again modeled by the diffusion equation. At the interfaces between liquid film and vapor, we impose the energy conservation. We use  $T_{w0}, T_{w1}$  to denote wall temperature at hot and cold wall respectively, and  $T_{l0}$  and  $T_{l1}$  corresponding the liquid-vapor interface temperatures.

The temperature variation within the liquid film is modeled by heat conduction, which had been justified<sup>58,61</sup>, and the solution linearly interpolate the wall and the liquid interface temperature. Accordingly, the vapor heat flux at the evaporating and condensing are, respectively

$$q_{l0} = k_w \frac{T_{w0} - T_{l0}}{d_0} - \dot{m}\Gamma, \quad q_{l1} = k_w \frac{T_{l1} - T_{w1}}{d_1} - \dot{m}\Gamma, \quad (1)$$

where  $k_w = 0.6 \text{W} \cdot \text{m}^{-1} \cdot \text{K}^{-1}$  is heat conductivity of the liquid,  $d_0$  and  $d_1$  are thicknesses of liquid layers. Since liquid undergoes phase changes from liquid to vapor, the heat flux also composes a component  $\dot{m}\Gamma$  with  $\Gamma = 2.3 \text{MJ} \cdot \text{kg}^{-1}$  denoting the latent heat for the phase change and  $\dot{m}$  representing the mass flux.

In the vapor region, we deploy the steady BGK model to describe the gas dynamics. Since our system enjoys planetary symmetry, we assume that the drift velocity is only in the direction perpendicular to wall, and the 1D-space 3D-velocity model reads

$$v_1 \partial_x f = \frac{1}{\tau} (\mathcal{M}[f] - f), \quad x \in [0, L], v = (v_1, v_2, v_3) \in \mathbb{R}^3, \quad (2)$$

here  $L$  represents the thickness of vapor region,  $f = f(x, v_1, v_2, v_3)$  is the mass density of gas molecules at location  $x$  with velocity  $(v_1, v_2, v_3)$ ,  $\tau$  is the relaxation time which is treated as a constant here and  $\mathcal{M}[f]$  represents the local equilibrium (displaced Maxwellian):

$$\mathcal{M}[f] = \frac{\rho}{(2\pi k_B T / m_0)^{3/2}} e^{-\frac{(v_1 - u)^2 + v_2^2 + v_3^2}{2k_B T / m_0}}, \quad (3)$$

where  $k_B$  is the Boltzmann constant,  $m_0$  is the molecular mass,  $\rho$  and  $u$  represent the local density and drift velocity respectively.

We provide the nondimensionalization for this model, and investigate its boundary conditions that interact with the diffusion models for the liquid.

## A. Nondimensionalization

We denote  $L$  the thickness of vapor region,  $u_0$  as the typical particle velocity, and introduce normalized variables  $\hat{x} := x/L$ ,  $\hat{v}_i := v_i/u_0$ ,  $\hat{\theta} := \frac{k_B T}{m_0 u_0^2}$ , where  $u_0 = 200 \text{m} \cdot \text{s}^{-1}$ , and thus on these new variables,  $\hat{f}(\hat{x}, \hat{v}_i) = f(L\hat{x}, u_0\hat{v}_i) = f(x, v)$  satisfies the dimensionless BGK equation:

$$\hat{v}_1 \partial_{\hat{x}} \hat{f}(\hat{x}, \hat{v}_i) = -\frac{1}{\tau u_0 / L} \left( \hat{f}(\hat{x}, \hat{v}_i) - \mathcal{M}[\hat{f}] \right), \quad (4)$$

for  $0 < \hat{x} < 1, \hat{v} \in \mathbb{R}^3$  and we denote  $Kn := \frac{\tau u_0}{L}$  as the Knudsen number that represents the ratio between molecular mean free path and the characteristic length of vapor region. For simplicity of notations, we will drop all hats for nondimensional variables from now on. Furthermore, due to the assumption of symmetry as in (3) that drift velocity  $u$  is in the first direction, we can reduce the original velocity space to  $1D$  as in Aoki et al.<sup>14</sup>, by multiplying 1 and  $(v_2^2 + v_3^2)$  to both sides in (4) then integrate over  $v_2$  and  $v_3$ . That is, we define new density functions:

$$g(x, v_1) := \int_{\mathbb{R}^2} f dv_2 dv_3, \quad (5)$$

$$h(x, v_1) := \int_{\mathbb{R}^2} (v_2^2 + v_3^2) f dv_2 dv_3. \quad (6)$$

And we obtain the following system in nondimensional variables:

$$v_1 \partial_x g = -\frac{1}{Kn} \left( g - \frac{\rho}{\sqrt{2\pi\theta}} e^{-\frac{(v_1-u)^2}{2\theta}} \right), \quad (7)$$

$$v_1 \partial_x h = -\frac{1}{Kn} \left( h - \frac{2\rho\theta}{\sqrt{2\pi\theta}} e^{-\frac{(v_1-u)^2}{2\theta}} \right), \quad (8)$$

The macroscopic quantities of density, average velocity and normalized temperature, are defined by:

$$\rho(x) := \int_{\mathbb{R}} g dv_1, \quad (9)$$

$$u(x) := \frac{1}{\rho} \int_{\mathbb{R}} v_1 g dv_1, \quad (10)$$

$$\theta(x) := \frac{1}{3\rho} \int_{\mathbb{R}} ((v_1 - u)^2 g + h) dv_1. \quad (11)$$

The equation is equipped with boundary conditions. We denote  $\phi_0$  and  $\phi_1$  as the inflow boundary condition prepared at the hot and cold walls respectively, and  $\alpha$  as the accommodation coefficient to include the specular reflection of  $f$ , i.e.

$$\begin{aligned} f(x=0, v_1 > 0) &= \alpha\phi_0 + (1-\alpha)f(x=0, -v_1), \\ f(x=1, v_1 < 0) &= \alpha\phi_1 + (1-\alpha)f(x=1, -v_1). \end{aligned} \quad (12)$$

The boundary conditions for  $g$  and  $h$  are accordingly determined by their definitions, together with these we arrive at the final model (13) and (14).

$$\begin{cases} v_1 \partial_x g = -\frac{1}{Kn} \left( g - \frac{\rho}{\sqrt{2\pi\theta}} e^{-\frac{(v_1-u)^2}{2\theta}} \right), \\ g(x=0, v_1 > 0) = \alpha\phi_0^g + (1-\alpha)g(x=0, -v_1), \\ g(x=1, v_1 < 0) = \alpha\phi_1^g + (1-\alpha)g(x=1, -v_1), \end{cases} \quad (13)$$

$$\begin{cases} v_1 \partial_x h = -\frac{1}{Kn} \left( h - \frac{2\rho\theta}{\sqrt{2\pi\theta}} e^{-\frac{(v_1-u)^2}{2\theta}} \right), \\ h(x=0, v_1 > 0) = \alpha\phi_0^h + (1-\alpha)h(x=0, -v_1), \\ h(x=1, v_1 < 0) = \alpha\phi_1^h + (1-\alpha)h(x=1, -v_1). \end{cases} \quad (14)$$

When  $\alpha = 1$  the boundary condition is reduced to Dirichlet type, whereas  $\alpha = 0$  corresponds to only specular reflection.

As a consequence of the model above, we can compute the dimensionless mass flux and energy flux in the vapor region:

$$\dot{m}(x) = \int_{\mathbb{R}^3} v_1 f dv = \int_{\mathbb{R}} v_1 g dv_1, \quad (15)$$

$$j_e(x) = \int_{\mathbb{R}^3} v_1 \frac{|v|^2}{2} f dv = \int_{\mathbb{R}} \frac{v_1^3}{2} g dv_1 + \int_{\mathbb{R}} \frac{v_1}{2} h dv_1. \quad (16)$$

## B. Decomposition of Energy Flux

Total energy flux can be decomposed into heat flux, enthalpy flux and kinetic energy flux. This can be seen from the steady state BGK model (4), or equivalently (7) and (8).

More specifically, BGK model preserves energy, meaning:

$$\partial_x j_e = \partial_x \int_{\mathbb{R}^3} v_1 \frac{|v|^2}{2} f dv = 0. \quad (17)$$

Expanding this term with respect to  $u$ , the molecular average velocity:

$$\begin{aligned} j_e &= \frac{1}{2} \int_{\mathbb{R}^3} (v_1 - u)((v_1 - u)^2 + v_2^2 + v_3^2) f dv \\ &\quad + \frac{1}{2} \int_{\mathbb{R}^3} (2(v_1 - u) + u)u^2 f dv \\ &\quad + \frac{1}{2} \int_{\mathbb{R}^3} (v_1 - u)(2u(v_1 - u) + u^2) f dv \\ &\quad + \frac{1}{2} \int_{\mathbb{R}^3} u((v_1 - u)^2 + v_2^2 + v_3^2) f dv. \end{aligned} \quad (18)$$

The first term is the microscopic expression of heat flux<sup>59</sup>:

$$q(x) = \frac{1}{2} \int_{\mathbb{R}^3} (v_1 - u_1)((v_1 - u_1)^2 + v_2^2 + v_3^2) f dv, \quad (19)$$

and the second term

$$\frac{1}{2} \int_{\mathbb{R}^3} (2(v_1 - u) + u)u^2 f dv = \frac{1}{2}\rho u^3, \quad (20)$$

is understood as kinetic energy flux. To interpret the last two terms, we notice:

$$\int_{\mathbb{R}^3} (v_1 - u)(2u(v_1 - u) + u^2)f \, dv = 2u(\rho\theta) = 2up, \quad (21)$$

where  $p$  is the local pressure according to ideal gas law, making this term representing the pressure work flux, and

$$\int_{\mathbb{R}^3} u((v_1 - u)^2 + v_2^2 + v_3^2)f \, dv = 2u\rho e, \quad (22)$$

represents the internal energy flux with  $e$  denoting the internal energy. Considering enthalpy  $h = p/\rho + e$ , we can understand the last two terms together as the enthalpy flux  $\rho uh$ . Therefore:

$$\partial_x j_e = \partial_x \left( q + \rho uh + \frac{1}{2}\rho u^3 \right) = 0. \quad (23)$$

### C. Coupling of models

At the interface of liquid film and water vapor, we couple the diffusion equation for the liquid and the BGK equation for the vapor through energy conservation.

#### 1. Liquid to vapor

Liquid temperature at the interface provides boundary condition for the BGK model. More specifically,  $\phi_{0,1}$  are assumed to be the local equilibrium under saturation temperature  $T_{l0}, T_{l1}$  respectively, or in dimensionless variables  $\theta_{l0}, \theta_{l1}$ ,

$$\phi_0 = \frac{\rho_0}{(2\pi\theta_{l0})^{3/2}} e^{-\frac{v_1^2+v_2^2+v_3^2}{2\theta_{l0}}}, \quad \phi_1 = \frac{\rho_1}{(2\pi\theta_{l1})^{3/2}} e^{-\frac{v_1^2+v_2^2+v_3^2}{2\theta_{l1}}}, \quad (24)$$

and hence

$$\phi_i^g = \frac{\rho_i}{\sqrt{2\pi\theta_{li}}} e^{-\frac{v_1^2}{2\theta_{li}}}, \quad \phi_i^h = \frac{2\rho_i\theta_{li}}{\sqrt{2\pi\theta_{li}}} e^{-\frac{v_1^2}{2\theta_{li}}}, \quad i = 0, 1, \quad (25)$$

where the interface densities  $\rho_{0,1}$  are the dimensionless densities  $\rho_{0,1} = \rho(T_{l0,l1})/\rho_r$ , with  $\rho(T)$  being determined by the Clausius-Clapeyron equation for saturated gas:

$$\rho = \frac{\rho_r T_r}{T} \exp \left( -\frac{\Gamma}{R} \left( \frac{1}{T} - \frac{1}{T_r} \right) \right), \quad (26)$$

where  $R$  is the ideal gas constant,  $\Gamma$  is the latent heat, and  $(\rho_r, T_r)$  is the density and temperature at some reference point, and take on fixed values for specific material.

For example, for water close to room temperature, setting  $T_r = 273\text{K}$ , this nonlinear relation is approximately<sup>58</sup>:

$$\rho = 5.018 + 0.3232\Delta T + 8.1847 \times 10^{-3}(\Delta T)^2 + 3.1243 \times 10^{-4}(\Delta T)^3, \quad (27)$$

where  $\Delta T = T - 273$  represents the temperature difference between absolute temperature and  $T_r$ .

## 2. Energy balance

The vapor BGK model provides boundary condition for liquid as well. This condition comes in the form of energy conservation.

Recall (1) derived from the heat equation for the liquid, and (16) derived from BGK model for vapor, we equip the two sources of energy flux to obtain:

$$\begin{cases} k_w \frac{T_{w0} - T_{l0}}{d_0} - \dot{m}(x=0)\Gamma = j_e(x=0), \\ k_w \frac{T_{l1} - T_{w1}}{d_1} - \dot{m}(x=L)\Gamma = j_e(x=L). \end{cases} \quad (28)$$

Noting that  $j_e$  and  $\dot{m}$  are solutions to the BGK model (13) (14), hence (28) presents a highly nonlinear convoluted system. We solve it in an iterated scheme. At the  $n$ -th iteration, we utilize the current saturation temperature  $(T_{l0}^n, T_{l1}^n)$  to solve (13) (14) under the boundary conditions. The output of the solutions, denoted by  $g^n$  and  $h^n$  are used to compute  $\dot{m}^n, j_e^n$  in (28), or equivalently, to update the guess as in (29).

$$\begin{cases} T_{l0}^{n+1} = T_{w0} - \frac{d_0}{k_w}\Gamma \int_{\mathbb{R}} v_1 g^n(x=0) dv_1 - \frac{d_0}{k_w} \frac{1}{2} \int_{\mathbb{R}} v_1^3 g^n(x=0) dv_1 - \frac{d_0}{k_w} \frac{1}{2} \int_{\mathbb{R}} v_1 h^n(x=0) dv_1, \\ T_{l1}^{n+1} = T_{w1} + \frac{d_1}{k_w}\Gamma \int_{\mathbb{R}} v_1 g^n(x=L) dv_1 + \frac{d_1}{k_w} \frac{1}{2} \int_{\mathbb{R}} v_1^3 g^n(x=L) dv_1 + \frac{d_1}{k_w} \frac{1}{2} \int_{\mathbb{R}} v_1 h^n(x=L) dv_1. \end{cases} \quad (29)$$

## D. Semi-continuum solution

The semi-continuum solution is based on the asymptotic computations in the Supplementary materials, introduced by Chen<sup>55</sup>. The constant pressure specific heat and vapor heat conductivity are computed based on the properties of monoatomic gas<sup>62</sup>:  $c_p = \frac{5}{2} \frac{k_B}{m_0} = 1153 \text{ J}\cdot\text{K}^{-1}\cdot\text{kg}^{-1}$ ,  $k_v = \frac{5}{2}\tau \left(\frac{k_B}{m_0}\right)^2 \rho T = 0.0036 \text{ W}\cdot\text{K}^{-1}\cdot\text{m}^{-1}$ . We choose  $\tau = 0.5 \times 10^{-9} \text{ s}$ ,  $\rho T =$

$13.6 \text{ kg} \cdot \text{m}^{-3} \cdot \text{K}$  since the pressure in the vapor region is constant in the semi-continuum approximation.

#### IV. SUPPLEMENTARY MATERIAL

In the supplementary material, we provide a detailed asymptotic calculation for small  $Kn$ , including the derivation of mass flux and energy flux in the bulk region and near the interfaces, as well as a review of the semi-continuum solution introduced by Chen<sup>55</sup>. In addition, we summarize the units of several key physical quantities used throughout the paper.

#### ACKNOWLEDGMENTS

P.C. and Q.L. acknowledge support from NSF-DMS- 2308440. G.C. acknowledges support from MIT Bose Award and UMRP.

#### CONFLICT OF INTEREST

The authors have no conflicts to disclose.

#### AUTHOR CONTRIBUTIONS

Conceptualization: G.C.; Data curation: P.C., Q.L. and G.C.; Formal analysis: P.C., Q.L. and G.C. ; Investigation: P.C., Q.L. and G.C.; Methodology: G.C., Q.L. and P.C.; Software: P.C.; Writing – original draft: G.C., Q.L. and P.C..

#### REFERENCES

- <sup>1</sup>A. Bejan, *Advanced Engineering Thermodynamics* (John Wiley & Sons, Ltd, 2016) <https://onlinelibrary.wiley.com/doi/pdf/10.1002/9781119245964.fmatter>.
- <sup>2</sup>M. J. Moran, *Availability analysis : a guide to efficient energy use*, corr. ed. ed. (ASME Press, New York, 1989).

- <sup>3</sup>H. Hertz, “Ueber die verdunstung der flüssigkeiten, insbesondere des quecksilbers, im luftleeren raume,” *Annalen der Physik* **253**, 177–193 (1882), <https://onlinelibrary.wiley.com/doi/pdf/10.1002/andp.18822531002>.
- <sup>4</sup>M. Knudsen, “Die maximale verdampfungsgeschwindigkeit des quecksilbers,” *Annalen der Physik* **352**, 697–708 (1915), <https://onlinelibrary.wiley.com/doi/pdf/10.1002/andp.19153521306>.
- <sup>5</sup>R. W. Schrage, *A Theoretical Study of Interphase Mass Transfer* (Columbia University Press, New York Chichester, West Sussex, 1953).
- <sup>6</sup>V. Carey, *Liquid-Vapor Phase-Change Phenomena: An Introduction to the Thermophysics of Vaporization and Condensation Processes in Heat Transfer Equipment, Third Edition (3rd ed.)* (CRC Press, 2020) <https://doi.org/10.1201/9780429082221>.
- <sup>7</sup>Y. Pao, “Temperature and Density Jumps in the Kinetic Theory of Gases and Vapors,” *The Physics of Fluids* **14**, 1340–1346 (1971), [https://pubs.aip.org/aip/pfl/article-pdf/14/7/1340/12445720/1340.1\\_online.pdf](https://pubs.aip.org/aip/pfl/article-pdf/14/7/1340/12445720/1340.1_online.pdf).
- <sup>8</sup>Y. Pao, “Application of kinetic theory to the problem of evaporation and condensation,” *The Physics of Fluids* **14**, 306–312 (1971).
- <sup>9</sup>Y. Sone, T. Ohwada, and K. Aoki, “Evaporation and condensation on a plane condensed phase: Numerical analysis of the linearized boltzmann equation for hard-sphere molecules,” *Physics of Fluids A: Fluid Dynamics* **1**, 1398–1405 (1989), [https://pubs.aip.org/aip/pof/article-pdf/1/8/1398/12389154/1398.1\\_online.pdf](https://pubs.aip.org/aip/pof/article-pdf/1/8/1398/12389154/1398.1_online.pdf).
- <sup>10</sup>K. Aoki and N. Masukawa, “Gas flows caused by evaporation and condensation on two parallel condensed phases and the negative temperature gradient: Numerical analysis by using a nonlinear kinetic equation,” *Physics of Fluids* **6**, 1379–1395 (1994).
- <sup>11</sup>C. Cercignani, W. Fiszdon, and A. Frezzotti, “The paradox of the inverted temperature profiles between an evaporating and a condensing surface,” *The Physics of Fluids* **28**, 3237–3240 (1985), [https://pubs.aip.org/aip/pfl/article-pdf/28/11/3237/12272873/3237.1\\_online.pdf](https://pubs.aip.org/aip/pfl/article-pdf/28/11/3237/12272873/3237.1_online.pdf).
- <sup>12</sup>J. Cipolla, J. W., H. Lang, and S. K. Loyalka, “Kinetic theory of condensation and evaporation. ii,” *The Journal of Chemical Physics* **61**, 69–77 (1974), [https://pubs.aip.org/aip/jcp/article-pdf/61/1/69/18891265/69.1\\_online.pdf](https://pubs.aip.org/aip/jcp/article-pdf/61/1/69/18891265/69.1_online.pdf).
- <sup>13</sup>A. Frezzotti, “A numerical investigation of the steady evaporation of a polyatomic gas,” *European Journal of Mechanics - B/Fluids* **26**, 93–104 (2007).

- <sup>14</sup>K. Aoki, Y. Sone, and T. Yamada, “Numerical analysis of gas flows condensing on its plane condensed phase on the basis of kinetic theory,” *Phys. Fluids* **2**, 1867–1878 (1990).
- <sup>15</sup>L. D. Koffman, M. S. Plesset, and L. Lees, “Theory of evaporation and condensation,” *The Physics of Fluids* **27**, 876–880 (1984), [https://pubs.aip.org/aip/pfl/article-pdf/27/4/876/12518579/876\\_1\\_online.pdf](https://pubs.aip.org/aip/pfl/article-pdf/27/4/876/12518579/876_1_online.pdf).
- <sup>16</sup>T. Ytrehus and S. Østmo, “Kinetic theory approach to interphase processes,” *International Journal of Multiphase Flow* **22**, 133–155 (1996).
- <sup>17</sup>E. Aursand and T. Ytrehus, “Comparison of kinetic theory evaporation models for liquid thin-films,” *International Journal of Multiphase Flow* **116**, 67–79 (2019).
- <sup>18</sup>G. Vaartstra, Z. Lu, J. H. Lienhard, and E. N. Wang, “Revisiting the schrage equation for kinetically limited evaporation and condensation,” *Journal of Heat Transfer* **144**, 080802 (2022), [https://asmedigitalcollection.asme.org/heattransfer/article-pdf/144/8/080802/6882851/ht\\_144\\_08\\_080802.pdf](https://asmedigitalcollection.asme.org/heattransfer/article-pdf/144/8/080802/6882851/ht_144_08_080802.pdf).
- <sup>19</sup>P. Jafari, A. Masoudi, P. Irajizad, M. Nazari, V. Kashyap, B. Eslami, and H. Ghasemi, “Evaporation mass flux: A predictive model and experiments,” *Langmuir* **34**, 11676–11684 (2018).
- <sup>20</sup>A. Frezzotti, P. Grosfils, and S. Toxvaerd, “Evidence of an inverted temperature gradient during evaporation/condensation of a lennard-jones fluid,” *Physics of Fluids* **15**, 2837–2842 (2003), [https://pubs.aip.org/aip/pof/article-pdf/15/10/2837/19131653/2837\\_1\\_online.pdf](https://pubs.aip.org/aip/pof/article-pdf/15/10/2837/19131653/2837_1_online.pdf).
- <sup>21</sup>R. Meland, A. Frezzotti, T. Ytrehus, and B. Hafskjold, “Nonequilibrium molecular-dynamics simulation of net evaporation and net condensation, and evaluation of the gas-kinetic boundary condition at the interphase,” *Physics of Fluids* **16**, 223–243 (2004), [https://pubs.aip.org/aip/pof/article-pdf/16/2/223/19097705/223\\_1\\_online.pdf](https://pubs.aip.org/aip/pof/article-pdf/16/2/223/19097705/223_1_online.pdf).
- <sup>22</sup>A. Chandra and P. Keblinski, “Investigating the validity of schrage relationships for water using molecular dynamics simulations,” *The Journal of Chemical Physics* **153**, 124505 (2020), [https://pubs.aip.org/aip/jcp/article-pdf/doi/10.1063/5.0018726/14755787/124505\\_1\\_online.pdf](https://pubs.aip.org/aip/jcp/article-pdf/doi/10.1063/5.0018726/14755787/124505_1_online.pdf).
- <sup>23</sup>E. Bird, J. Gutierrez Plascencia, P. Keblinski, and Z. Liang, “Molecular simulation of steady-state evaporation and condensation of water in air,” *International Journal of Heat and Mass Transfer* **184**, 122285 (2022).

- <sup>24</sup>A. Rokoni and Y. Sun, “Probing the temperature profile across a liquid–vapor interface upon phase change,” *The Journal of Chemical Physics* **153**, 144706 (2020), [https://pubs.aip.org/aip/jcp/article-pdf/doi/10.1063/5.0024722/13373369/144706\\_1\\_online.pdf](https://pubs.aip.org/aip/jcp/article-pdf/doi/10.1063/5.0024722/13373369/144706_1_online.pdf).
- <sup>25</sup>V. V. Zhakhovskii and S. I. Anisimov, “Molecular-dynamics simulation of evaporation of a liquid,” *Journal of Experimental and Theoretical Physics* **84**, 734–745 (1997).
- <sup>26</sup>V. V. Zhakhovsky, A. P. Kryukov, V. Y. Levashov, I. N. Shishkova, and S. I. Anisimov, “Mass and heat transfer between evaporation and condensation surfaces: Atomistic simulation and solution of boltzmann kinetic equation,” *Proc Natl Acad Sci U S A* **116**, 18209–18217 (2018).
- <sup>27</sup>M. Kon, K. Kobayashi, and M. Watanabe, “Liquid temperature dependence of kinetic boundary condition at vapor–liquid interface,” *International Journal of Heat and Mass Transfer* **99**, 317–326 (2016).
- <sup>28</sup>R. Meland, “Molecular dynamics simulation of the inverted temperature gradient phenomenon,” *Physics of Fluids* **15**, 3244–3247 (2003), [https://pubs.aip.org/aip/pof/article-pdf/15/10/3244/19131701/3244\\_1\\_online.pdf](https://pubs.aip.org/aip/pof/article-pdf/15/10/3244/19131701/3244_1_online.pdf).
- <sup>29</sup>A. Tokunaga and T. Tsuruta, “Nonequilibrium molecular dynamics study on energy accommodation coefficient on condensing liquid surface—molecular boundary conditions for heat and mass transfer,” *Physics of Fluids* **32**, 112011 (2020), [https://pubs.aip.org/aip/pof/article-pdf/doi/10.1063/5.0027945/19777215/112011\\_1\\_online.pdf](https://pubs.aip.org/aip/pof/article-pdf/doi/10.1063/5.0027945/19777215/112011_1_online.pdf).
- <sup>30</sup>Y. Sone and Y. Onishi, “Kinetic Theory of Evaporation and Condensation, Hydrodynamic Equation and Slip Boundary Condition,” *Journal of the Physical Society of Japan* **44**, 1981–1994 (1978).
- <sup>31</sup>Y. Sone, S. Takata, and F. Golse, “Notes on the boundary conditions for fluid-dynamic equations on the interface of a gas and its condensed phase,” *Physics of Fluids* **13**, 324–334 (2001), [https://pubs.aip.org/aip/pof/article-pdf/13/1/324/19034403/324\\_1\\_online.pdf](https://pubs.aip.org/aip/pof/article-pdf/13/1/324/19034403/324_1_online.pdf).
- <sup>32</sup>J. Barrett and C. Clement, “Kinetic evaporation and condensation rates and their coefficients,” *Journal of Colloid and Interface Science* **150**, 352–364 (1992).
- <sup>33</sup>A. Frezzotti, “Boundary conditions at the vapor-liquid interface,” *Physics of Fluids* **23**, 030609 (2011), [https://pubs.aip.org/aip/pof/article-pdf/doi/10.1063/1.3567001/15747996/030609\\_1\\_online.pdf](https://pubs.aip.org/aip/pof/article-pdf/doi/10.1063/1.3567001/15747996/030609_1_online.pdf).

- <sup>34</sup>L. E. R. R. Y. Kucherov, “On hydrodynamic boundary conditions for evaporation and condensation.” *J. Exptl. Theoret. Phys. (U.S.S.R.)* **37**, 125–126 (1960).
- <sup>35</sup>K. Aoki and C. Cercignani, “Evaporation and condensation on two parallel plates at finite Reynolds numbers,” *Phys. Fluids* **26**, 1163–1164 (1983).
- <sup>36</sup>E. Gatapova, I. Graur, F. Sharipov, and O. Kabov, “The temperature and pressure jumps at the vapor–liquid interface: Application to a two-phase cooling system,” *International Journal of Heat and Mass Transfer* **83**, 235–243 (2015).
- <sup>37</sup>G. Fang and C. A. Ward, “Temperature measured close to the interface of an evaporating liquid,” *Phys. Rev. E* **59**, 417–428 (1999).
- <sup>38</sup>C. A. Ward and D. Stanga, “Interfacial conditions during evaporation or condensation of water,” *Phys. Rev. E* **64**, 051509 (2001).
- <sup>39</sup>A. J. H. McGaughey and C. A. Ward, “Temperature discontinuity at the surface of an evaporating droplet,” *Journal of Applied Physics* **91**, 6406–6415 (2002), [https://pubs.aip.org/aip/jap/article-pdf/91/10/6406/19206657/6406\\_1\\_online.pdf](https://pubs.aip.org/aip/jap/article-pdf/91/10/6406/19206657/6406_1_online.pdf).
- <sup>40</sup>V. Badam, V. Kumar, F. Durst, and K. Danov, “Experimental and theoretical investigations on interfacial temperature jumps during evaporation,” *Experimental Thermal and Fluid Science* **32**, 276–292 (2007).
- <sup>41</sup>F. Duan, C. A. Ward, V. K. Badam, and F. Durst, “Role of molecular phonons and interfacial-temperature discontinuities in water evaporation,” *Phys. Rev. E* **78**, 041130 (2008).
- <sup>42</sup>M. A. Kazemi, D. S. Nobes, and J. A. W. Elliott, “Experimental and numerical study of the evaporation of water at low pressures,” *Langmuir* **33**, 4578–4591 (2017).
- <sup>43</sup>H. Ghasemi and C. A. Ward, “Mechanism of sessile water droplet evaporation: Kapitza resistance at the Solid–Liquid interface,” *J. Phys. Chem. C* **115**, 21311–21319 (2011).
- <sup>44</sup>H. Ghasemi and C. A. Ward, “Energy transport by thermocapillary convection during sessile-water-droplet evaporation,” *Phys. Rev. Lett.* **105**, 136102 (2010).
- <sup>45</sup>E. Gatapova, I. Graur, O. Kabov, V. Aniskin, M. Filipenko, F. Sharipov, and L. Tadriss, “The temperature jump at water – air interface during evaporation,” *International Journal of Heat and Mass Transfer* **104**, 800–812 (2017).
- <sup>46</sup>Z. Zhu and Q.-S. Liu, “Interfacial temperature discontinuities in a thin liquid layer during evaporation,” *Microgravity Science and Technology* **25**, 243–249 (2013).

- <sup>47</sup>Z.-Q. Zhu, Q.-S. Liu, and J.-C. Xie, “Experimental study on the combined evaporation effect and thermocapillary convection in a thin liquid layer,” *Microgravity Science and Technology* **21**, 241–246 (2009).
- <sup>48</sup>C. Buffone and K. Sefiane, “Ir measurements of interfacial temperature during phase change in a confined environment,” *Experimental Thermal and Fluid Science* **29**, 65–74 (2004).
- <sup>49</sup>M. A. Kazemi, D. S. Nobes, and J. A. W. Elliott, “Effect of the thermocouple on measuring the temperature discontinuity at a Liquid–Vapor interface,” *Langmuir* **33**, 7169–7180 (2017).
- <sup>50</sup>E. Y. Gatapova, “Evaporation into half-space: Experiments with water at the molecular mean free path scale,” *Physics of Fluids* **36**, 091707 (2024), [https://pubs.aip.org/aip/pof/article-pdf/doi/10.1063/5.0228893/20167991/091707\\_1\\_5.0228893.pdf](https://pubs.aip.org/aip/pof/article-pdf/doi/10.1063/5.0228893/20167991/091707_1_5.0228893.pdf).
- <sup>51</sup>S. Popov, A. Melling, F. Durst, and C. Ward, “Apparatus for investigation of evaporation at free liquid–vapour interfaces,” *International Journal of Heat and Mass Transfer* **48**, 2299–2309 (2005).
- <sup>52</sup>P. Jafari, A. Amritkar, and H. Ghasemi, “Temperature discontinuity at an evaporating water interface,” *The Journal of Physical Chemistry C* **124**, 1554–1559 (2020), <https://doi.org/10.1021/acs.jpcc.9b10838>.
- <sup>53</sup>C. A. Ward and G. Fang, “Expression for predicting liquid evaporation flux: Statistical rate theory approach,” *Phys. Rev. E* **59**, 429–440 (1999).
- <sup>54</sup>D. Bedeaux, L. Hermans, and T. Ytrehus, “Slow evaporation and condensation,” *Physica A: Statistical Mechanics and its Applications* **169**, 263–280 (1990).
- <sup>55</sup>G. Chen, “On the molecular picture and interfacial temperature discontinuity during evaporation and condensation,” *International Journal of Heat and Mass Transfer* **191** (2022).
- <sup>56</sup>G. Chen, “Interfacial cooling and heating, temperature discontinuity and inversion in evaporation and condensation,” *International Journal of Heat and Mass Transfer* **218** (2024).
- <sup>57</sup>G. Chen, “Interfacial temperature and density discontinuities for phase-change heat transfer with non-condensable gas,” arXiv:2501.17058 [Preprint] (2025).
- <sup>58</sup>G. Chen, “On paradoxical phenomena during evaporation and condensation between two parallel plates,” *The Journal of Chemical Physics* **159**, 151101 (2023).

- <sup>59</sup>W. Vincenti and C. Kruger, *Introduction to Physical Gas Dynamics*, @Interscience tracts on physics and astronomy (John Wiley & Sons, 1965).
- <sup>60</sup>G. D. Mahan, “Thermionic refrigeration,” *Journal of Applied Physics* **76**, 4362–4366 (1994), [https://pubs.aip.org/aip/jap/article-pdf/76/7/4362/18670438/4362.1\\_online.pdf](https://pubs.aip.org/aip/jap/article-pdf/76/7/4362/18670438/4362.1_online.pdf).
- <sup>61</sup>P. Varilly and D. Chandler, “Water evaporation: A transition path sampling study,” *The Journal of Physical Chemistry B* **117**, 1419–1428 (2013), pMID: 23294322, <https://doi.org/10.1021/jp310070y>.
- <sup>62</sup>G. Chen, *Nanoscale energy transport and conversion : a parallel treatment of electrons, molecules, phonons, and photons* (Oxford University Press, New York, 2005).

## Appendix A: Asymptotic calculation for small $Kn$ .

Here we review the derivation of the semi-continuum solution. This framework couples the recently interfacial flux condition by Chen<sup>55</sup> and the classical Hertz-Knudsen formula.

### 1. Bulk vapor region

When Knudsen number  $Kn$  is small, we denote  $f_{Kn}$  as the solution to the dimensionless BGK equation:

$$v_1 \partial_x f(x, v_i) = -\frac{1}{Kn} \left( f(x, v_i) - \frac{\rho}{(2\pi\theta)^{3/2}} e^{-\frac{(v_1-u)^2+v_2^2+v_3^2}{2\theta}} \right), \quad 0 < x < 1, \hat{v} \in \mathbb{R}^3, \quad (\text{A1})$$

We will derive the asymptotic mass flux and the energy flux in terms of  $f_{Kn}$ , since the macroscopic quantities obtained from  $g_{Kn}$  and  $h_{Kn}$  are equivalent to those derived from  $f_{Kn}$ . One can write the first order approximation solution to steady BGK (A1):

$$f_{Kn}(x, v) \approx f_0(x, v) - Kn(v_1 \partial_x f_0), \quad (\text{A2})$$

here  $f_0(x, v)$  is a local Maxwellian:

$$f_0(x, v) = \frac{\rho(x)}{(2\pi\theta(x))^{3/2}} e^{-\frac{(v_1-u(x))^2+v_2^2+v_3^2}{2\theta(x)}}, \quad (\text{A3})$$

and

$$\partial_x f_0(x, v) = \frac{\partial_x \rho}{\rho} f_0 + \partial_x u \frac{(v_1 - u)}{\theta} f_0 + \frac{1}{2} \frac{\partial_x \theta}{\theta} \left( \frac{(v_1 - u)^2 + v_2^2 + v_3^2}{\theta} - 3 \right) f_0. \quad (\text{A4})$$

Therefore, in the bulk vapor region, mass flux and energy flux are approximated by (A2) respectively as follows.

$$\dot{m}(x) \approx \int_{\mathbb{R}^3} v_1 f_{Kn} dv = \rho u - Kn [\partial_x \rho (\theta + u^2) + \partial_x u (2\rho u) + \partial_x \theta (\rho)], \quad (\text{A5})$$

$$\begin{aligned} q(x) &\approx \int_{\mathbb{R}^3} v_1 \frac{|v|^2}{2} f_{Kn} dv, \\ &= \frac{\rho u}{2} (5\theta + u^2) - Kn \left[ \partial_x \rho \left( \frac{5}{2}\theta^2 + 4u^2\theta + \frac{1}{2}u^4 \right) + \partial_x u (8\rho u\theta + 2\rho u^3) + \partial_x \theta (5\rho\theta + 4\rho u^2) \right]. \end{aligned} \quad (\text{A6})$$

Since the drift velocity is considered to be small in the bulk vapor region, mass flux and energy flux are further approximated by setting  $u^2 = 0$  and  $\partial_x u = 0$  in the above expressions( (A5) and (A6)),

$$\dot{m}(x) \approx \rho u - Kn [\partial_x \rho (\theta) + \partial_x \theta (\rho)], \quad (\text{A7})$$

$$q(x) \approx \left( \frac{5}{2} \rho u \theta \right) - Kn \left[ \partial_x \rho \left( \frac{5}{2} \theta^2 \right) + \partial_x \theta (5 \rho \theta) \right]. \quad (\text{A8})$$

To rewrite the above expressions into dimensional form, we recall the characteristic velocity  $u_0$ , Boltzmann constant  $k_B$ , molecular mass  $m_0$  and Knudsen number  $Kn = \frac{\tau u_0}{L}$ , then

$$\dot{m}(x) \approx \rho u - \tau \left[ \partial_x \rho \left( \frac{k_B T}{m_0} \right) + \partial_x T \left( \frac{k_B \rho}{m_0} \right) \right], \quad (\text{A9})$$

$$q(x) \approx \left( \frac{5}{2} \rho u \frac{k_B T}{m_0} \right) - \tau \left[ \partial_x \rho \left( \frac{5}{2} \left( \frac{k_B T}{m_0} \right)^2 \right) + \frac{k_B}{m_0} \partial_x T \left( 5 \rho \frac{k_B T}{m_0} \right) \right], \quad (\text{A10})$$

and hence

$$q(x) - \frac{5}{2} \frac{k_B}{m_0} \dot{m}(x) T = -\frac{5}{2} \tau \left( \frac{k_B}{m_0} \right)^2 \rho T \partial_x T. \quad (\text{A11})$$

Since  $\rho T$  is proportional to the constant pressure across the vapor region, according to the ideal gas law, the conservation of mass flux, energy flux leads to a transport-diffusion equation<sup>58</sup> that:

$$c_p \dot{m}(x) \partial_x T = \kappa \partial_x^2 T, \quad (\text{A12})$$

here we apply the definition of constant pressure heat capacity  $c_p := \frac{5}{2} \frac{k_B}{m_0}$ , and vapor thermal conductivity  $\kappa := \frac{5}{2} \tau \left( \frac{k_B}{m_0} \right)^2 \rho T$ .

## 2. Mass flux and energy flux near the interface

The semi-continuum solution ignores the boundary layer completely. Instead, it takes the Dirichlet boundary condition as the inflow and diffusion approximation solution (A2) as the outflow at the interface.

First we consider the liquid-vapor interface  $x = 0$ , and denote the saturated temperature of the liquid as  $T_{l0}$  (or  $\theta_{l0} = \frac{k_B}{m_0} \frac{T_{l0}}{(u_0)^2}$ ), bulk vapor temperature near  $x = 0$  as  $T_{v0}$  (or  $\theta_{v0} = \frac{k_B}{m_0} \frac{T_{v0}}{(u_0)^2}$ ), the saturated density at the interface as  $\rho_{l0}$ , and the bulk vapor density near  $x = 0$  as  $\rho_{v0}$ . Given the boundary condition with accommodation coefficient  $\alpha > 0$ :

$$f(x = 0, v_1 > 0) = \alpha \phi_0(v_1) + (1 - \alpha) f(x, -v_1), \quad \phi_0 = \frac{\rho_{l0}}{(2\pi\theta_{l0})^{3/2}} e^{-\frac{v_1^2 + v_2^2 + v_3^2}{2\theta_{l0}}}, \quad (\text{A13})$$

the incoming mass flux at interface is

$$\dot{m}_+(x = 0) := \int_{v_1 > 0} v_1 f(x = 0, v_1) dv = \alpha \int_{v_1 > 0} v_1 \phi_0(v) dv - (1 - \alpha) \dot{m}_-(x = 0), \quad (\text{A14})$$

The first term is the contribution from the imposed Dirichlet boundary condition that

$$\int_{v_1 > 0} v_1 \phi_0(v) dv = \int_0^\infty \frac{\rho_{l0}}{\sqrt{2\pi\theta_{l0}}} v_1 e^{-\frac{v_1^2}{2\theta_{l0}}} dv_1 = \frac{\rho_{l0}\theta_{l0}}{\sqrt{2\pi\theta_{l0}}}. \quad (\text{A15})$$

The outgoing mass flux takes in the reflection part, and is computed by the first order approximation (A2):

$$\dot{m}_-(x=0) := \int_{v_1 < 0} v_1 f_{Kn} dv \approx \int_{v_1 < 0} v_1 (f_0 - Kn(v_1 \partial_x f_0)) dv. \quad (\text{A16})$$

To explicitly compute each term, we list the following pre-calculations:

$$\begin{aligned} \int_{-\infty}^{-\frac{u_{v0}}{\sqrt{2\theta_{v0}}}} e^{-w^2} dw &= \frac{\sqrt{\pi}}{2} \left( 1 - \operatorname{erf} \left( \frac{u_{v0}}{\sqrt{2\theta_{v0}}} \right) \right), \\ \int_{-\infty}^{-\frac{u_{v0}}{\sqrt{2\theta_{v0}}}} w e^{-w^2} dw &= -\frac{1}{2} e^{-\frac{u_{v0}^2}{2\theta_{v0}}}, \\ \int_{-\infty}^{-\frac{u_{v0}}{\sqrt{2\theta_{v0}}}} w^2 e^{-w^2} dw &= \frac{u_{v0}}{2\sqrt{2\theta_{v0}}} e^{-\frac{u_{v0}^2}{2\theta_{v0}}} + \frac{\sqrt{\pi}}{4} \left( 1 - \operatorname{erf} \left( \frac{u_{v0}}{\sqrt{2\theta_{v0}}} \right) \right), \\ \int_{-\infty}^{-\frac{u_{v0}}{\sqrt{2\theta_{v0}}}} w^3 e^{-w^2} dw &= -\frac{u_{v0}^2}{4\theta_{v0}} e^{-\frac{u_{v0}^2}{2\theta_{v0}}} - \frac{1}{2} e^{-\frac{u_{v0}^2}{2\theta_{v0}}}, \\ \int_{-\infty}^{-\frac{u_{v0}}{\sqrt{2\theta_{v0}}}} w^4 e^{-w^2} dw &= \frac{u_{v0}^3}{4\theta_{v0}\sqrt{2\theta_{v0}}} e^{-\frac{u_{v0}^2}{2\theta_{v0}}} + \frac{3}{4} \frac{u_{v0}}{\sqrt{2\theta_{v0}}} e^{-\frac{u_{v0}^2}{2\theta_{v0}}} + \frac{3\sqrt{\pi}}{8} \left( 1 - \operatorname{erf} \left( \frac{u_{v0}}{\sqrt{2\theta_{v0}}} \right) \right), \\ \int_{-\infty}^{-\frac{u_{v0}}{\sqrt{2\theta_{v0}}}} w^5 e^{-w^2} dw &= -\frac{1}{2} \left[ \frac{u_{v0}^4}{4\theta_{v0}^2} + \frac{u_{v0}^2}{\theta_{v0}} + 2 \right] e^{-\frac{u_{v0}^2}{2\theta_{v0}}}, \\ \int_{-\infty}^{-\frac{u_{v0}}{\sqrt{2\theta_{v0}}}} w^6 e^{-w^2} dw &= \frac{1}{8} \frac{u_{v0}}{\sqrt{2\theta_{v0}}} e^{-\frac{u_{v0}^2}{2\theta_{v0}}} \left( \frac{u_{v0}^4}{\theta_{v0}^2} + \frac{5u_{v0}^2}{\theta_{v0}} + 15 \right) + \frac{15}{16} \sqrt{\pi} \left( 1 - \operatorname{erf} \left( \frac{u_{v0}}{\sqrt{2\theta_{v0}}} \right) \right). \end{aligned} \quad (\text{A17})$$

With these preparations, the first term from zeroth-order approximation  $f_0$  is:

$$\int_{v_1 < 0} v_1 f_0 dv = -\frac{\rho_{v0}\theta_{v0}}{\sqrt{2\pi\theta_{v0}}} e^{-\frac{u_{v0}^2}{2\theta_{v0}}} + \frac{\rho_{v0}u_{v0}}{2} \left( 1 - \operatorname{erf} \left( \frac{u_{v0}}{\sqrt{2\theta_{v0}}} \right) \right). \quad (\text{A18})$$

The second term related to density gradient  $\partial_x \rho_{v0}$  is:

$$\int_{v_1 < 0} v_1^2 \frac{\partial_x \rho_{v0}}{\rho_{v0}} f_0 dv = \partial_x \rho_{v0} \left[ -\frac{\theta_{v0}u_{v0}}{\sqrt{2\pi\theta_{v0}}} e^{-\frac{u_{v0}^2}{2\theta_{v0}}} + \frac{1}{2}(u_{v0}^2 + \theta_{v0}) \left( 1 - \operatorname{erf} \left( \frac{u_{v0}}{\sqrt{2\theta_{v0}}} \right) \right) \right], \quad (\text{A19})$$

The third term related to velocity gradient  $\partial_x u_{v0}$  is:

$$\int_{v_1 < 0} v_1^2 (v_1 - u_{v0}) \frac{\partial_x u_{v0}}{\theta_{v0}} f_0 dv = -(\partial_x u_{v0}) \frac{2\rho_{v0}\theta_{v0}}{\sqrt{2\pi\theta_{v0}}} e^{-\frac{u_{v0}^2}{2\theta_{v0}}} + (\partial_x u_{v0}) \rho_{v0} u_{v0} \left( 1 - \operatorname{erf} \left( \frac{u_{v0}}{\sqrt{2\theta_{v0}}} \right) \right), \quad (\text{A20})$$

The fourth term related to temperature gradient  $\partial_x \theta_{v0}$  is the sum of the following:

$$\begin{aligned}
 \frac{3}{2} \frac{\partial_x \theta_{v0}}{\theta_{v0}} \int_{v_1 < 0} v_1^2 f_0 dv &= -(\partial_x \theta_{v0}) \frac{3\rho_{v0} u_{v0}}{2\sqrt{2\pi}\theta_{v0}} e^{-\frac{u_{v0}^2}{2\theta_{v0}}} + (\partial_x \theta_{v0}) \rho_{v0} \left( \frac{3}{4} \frac{u_{v0}^2}{\theta_{v0}} + \frac{3}{4} \right) \left( 1 - \operatorname{erf} \left( \frac{u_{v0}}{\sqrt{2\theta_{v0}}} \right) \right), \\
 \frac{1}{2} \frac{\partial_x \theta_{v0}}{\theta_{v0}^2} \int_{v_1 < 0} v_1^2 (v_1 - u)^2 f_0 dv &= -(\partial_x \theta_{v0}) \frac{\rho_{v0} u_{v0}}{2\sqrt{2\pi}\theta_{v0}} e^{-\frac{u_{v0}^2}{2\theta_{v0}}} + (\partial_x \theta_{v0}) \rho_{v0} \left( \frac{1}{4} \frac{u_{v0}^2}{\theta_{v0}} + \frac{3}{4} \right) \left( 1 - \operatorname{erf} \left( \frac{u_{v0}}{\sqrt{2\theta_{v0}}} \right) \right), \\
 \frac{1}{2} \frac{\partial_x \theta_{v0}}{\theta_{v0}^2} \int_{v_1 < 0} v_1^2 v_2^2 f_0 dv &= -(\partial_x \theta_{v0}) \frac{\rho_{v0} u_{v0}}{2\sqrt{2\pi}\theta_{v0}} e^{-\frac{u_{v0}^2}{2\theta_{v0}}} + (\partial_x \theta_{v0}) \rho_{v0} \left( \frac{1}{4} \frac{u_{v0}^2}{\theta_{v0}} + \frac{1}{4} \right) \left( 1 - \operatorname{erf} \left( \frac{u_{v0}}{\sqrt{2\theta_{v0}}} \right) \right),
 \end{aligned} \tag{A21}$$

together with a correction of  $(\partial_x \theta_{v0}) \rho_{v0}$ . Thus the out-going mass flux is

$$\begin{aligned}
 \dot{m}_-(x=0) &= -\frac{\rho_{v0} \theta_{v0}}{\sqrt{2\pi}\theta_{v0}} e^{-\frac{u_{v0}^2}{2\theta_{v0}}} + \frac{\rho_{v0} u_{v0}}{2} \left( 1 - \operatorname{erf} \left( \frac{u_{v0}}{\sqrt{2\theta_{v0}}} \right) \right) \\
 &\quad + Kn(\partial_x \rho_{v0}) \frac{\theta_{v0} u_{v0}}{\sqrt{2\pi}\theta_{v0}} e^{-\frac{u_{v0}^2}{2\theta_{v0}}} - Kn(\partial_x \rho_{v0}) \frac{(u_{v0}^2 + \theta_{v0})}{2} \left( 1 - \operatorname{erf} \left( \frac{u_{v0}}{\sqrt{2\theta_{v0}}} \right) \right) \\
 &\quad + Kn(\partial_x u_{v0}) \frac{2\rho_{v0} \theta_{v0}}{\sqrt{2\pi}\theta_{v0}} e^{-\frac{u_{v0}^2}{2\theta_{v0}}} - Kn(\partial_x u_{v0}) \rho_{v0} u_{v0} \left( 1 - \operatorname{erf} \left( \frac{u_{v0}}{\sqrt{2\theta_{v0}}} \right) \right) \\
 &\quad - Kn(\partial_x \theta_{v0}) \rho_{v0} \frac{1}{2} \left( 1 - \operatorname{erf} \left( \frac{u_{v0}}{\sqrt{2\theta_{v0}}} \right) \right).
 \end{aligned} \tag{A22}$$

Typically drift velocity is much smaller than thermal velocity, so we let  $\partial_x u_{v0} = 0$ ,  $e^{-\frac{u_{v0}^2}{2\theta_{v0}}} = 0$ ,  $1 - \operatorname{erf} \left( \frac{u_{v0}}{\sqrt{2\theta_{v0}}} \right) = 1$ , then the out-going mass flux (A22) can be further approximated by

$$\dot{m}_-(x=0) \approx -\frac{\rho_{v0} \sqrt{\theta_{v0}}}{\sqrt{2\pi}} + \frac{1}{2} \dot{m}(x=0), \tag{A23}$$

where we recall the expression of approximated mass flux in the bulk vapor region near hot liquid (A7). Therefore by mass conservation:  $\dot{m}(x=0) = \dot{m}_+(x=0) + \dot{m}_-(x=0)$ ,

$$\dot{m}(x=0) \approx \frac{2\alpha}{2-\alpha} \frac{1}{\sqrt{2\pi}} \left( \rho_{l0} \sqrt{\theta_{l0}} - \rho_{v0} \sqrt{\theta_{v0}} \right). \tag{A24}$$

Similarly, the incoming energy flux at interface  $x=0$  satisfies:

$$q_+(x=0) := \int_{v_1 > 0} v_1 \frac{|v|^2}{2} f(x=0, v) dv = \frac{\alpha}{2} \int_{v_1 > 0} v_1 (v_1^2 + v_2^2 + v_3^2) \phi_0(v) dv - (1-\alpha) q_-(x=0). \tag{A25}$$

The contribution from Dirichlet data is

$$\int_{v_1 > 0} v_1 \frac{|v|^2}{2} \phi_0(v) dv = \frac{2\rho_{l0} \theta_{l0}^2}{\sqrt{2\pi}\theta_{l0}}. \tag{A26}$$

The outflow energy flux is again approximated by (A2):

$$q_-(x=0) \approx \int_{v_1 < 0} v_1 \frac{|v|^2}{2} (f_0 - Knv_1 \partial_x f_0) dv. \tag{A27}$$

The first term is from the local Maxwellian consisting of:

$$\begin{aligned} \int_{v_1 < 0} v_1^3 f_0 dv &= -\frac{\rho_{v0} \theta_{v0} (u_{v0}^2 + 2\theta_{v0})}{\sqrt{2\pi} \theta_{v0}} e^{-\frac{u_{v0}^2}{2\theta_{v0}}} + \frac{\rho_{v0} u_{v0} (3\theta_{v0} + u_{v0}^2)}{2} \left(1 - \operatorname{erf}\left(\frac{u_{v0}}{\sqrt{2\theta_{v0}}}\right)\right), \\ \int_{v_1 < 0} v_1 v_2^2 f_0 dv &= -\frac{\rho_{v0} \theta_{v0}^2}{\sqrt{2\pi} \theta_{v0}} e^{-\frac{u_{v0}^2}{2\theta_{v0}}} + \frac{\rho_{v0} u_{v0} \theta_{v0}}{2} \left(1 - \operatorname{erf}\left(\frac{u_{v0}}{\sqrt{2\theta_{v0}}}\right)\right). \end{aligned} \quad (\text{A28})$$

The second term related to density gradient  $\partial_x \rho_{v0}$  is from:

$$\begin{aligned} \int_{v_1 < 0} v_1^4 \frac{\partial_x \rho_{v0}}{\rho_{v0}} f_0 dv &= (\partial_x \rho_{v0}) \frac{\theta_{v0} u_{v0}}{\sqrt{2\pi} \theta_{v0}} (-u_{v0}^2 - 5\theta_{v0}) e^{-\frac{u_{v0}^2}{2\theta_{v0}}} \\ &\quad + (\partial_x \rho_{v0}) \left( \frac{u_{v0}^4}{2} + 3\theta_{v0} u_{v0}^2 + \frac{3\theta_{v0}^2}{2} \right) \left(1 - \operatorname{erf}\left(\frac{u_{v0}}{\sqrt{2\theta_{v0}}}\right)\right), \\ \int_{v_1 < 0} v_1^2 v_2^2 \frac{\partial_x \rho_{v0}}{\rho_{v0}} f_0 dv &= -(\partial_x \rho_{v0}) \frac{\theta_{v0}^2 u_{v0}}{\sqrt{2\pi} \theta_{v0}} e^{-\frac{u_{v0}^2}{2\theta_{v0}}} + (\partial_x \rho_{v0}) \left( \frac{\theta_{v0} u_{v0}^2}{2} + \frac{\theta_{v0}^2}{2} \right) \left(1 - \operatorname{erf}\left(\frac{u_{v0}}{\sqrt{2\theta_{v0}}}\right)\right). \end{aligned} \quad (\text{A29})$$

The third term takes the contribution about velocity gradient  $\partial_x u_{v0}$ :

$$\begin{aligned} \int_{v_1 < 0} v_1^4 (v_1 - u_{v0}) \frac{(\partial_x u_{v0})}{\theta_{v0}} f_0 dv &= (\partial_x u_{v0}) \frac{4\rho_{v0} \theta_{v0}}{\sqrt{2\pi} \theta_{v0}} (-u_{v0}^2 - 2\theta_{v0}) e^{-\frac{u_{v0}^2}{2\theta_{v0}}} \\ &\quad + (\partial_x u_{v0}) 2\rho_{v0} u_{v0} (3\theta_{v0} + u_{v0}^2) \left(1 - \operatorname{erf}\left(\frac{u_{v0}}{\sqrt{2\theta_{v0}}}\right)\right), \\ \int_{v_1 < 0} v_1^2 v_2^2 (v_1 - u_{v0}) \frac{(\partial_x u_{v0})}{\theta_{v0}} f_0 dv &= -(\partial_x u_{v0}) \frac{2\rho_{v0} \theta_{v0}^2}{\sqrt{2\pi} \theta_{v0}} e^{-\frac{u_{v0}^2}{2\theta_{v0}}} + (\partial_x u_{v0}) \rho_{v0} u_{v0} \theta_{v0} \left(1 - \operatorname{erf}\left(\frac{u_{v0}}{\sqrt{2\theta_{v0}}}\right)\right), \end{aligned} \quad (\text{A30})$$

The fourth term is about temperature gradient  $\partial_x \theta_{v0}$ :

$$\begin{aligned} \int_{v_1 < 0} v_1^4 (v_1 - u)^2 \frac{1}{2} \frac{\partial_x \theta_{v0}}{\theta_{v0}^2} f_0 dv &= (\partial_x \theta_{v0}) \rho_{v0} \left( \frac{15}{4} \theta_{v0} + \frac{1}{4} \frac{u_{v0}^4}{\theta_{v0}} + \frac{9}{2} u_{v0}^2 \right) \left(1 - \operatorname{erf}\left(\frac{u_{v0}}{\sqrt{2\theta_{v0}}}\right)\right) \\ &\quad - (\partial_x \theta_{v0}) \frac{\rho_{v0} u_{v0}}{2\sqrt{2\pi} \theta_{v0}} [17\theta_{v0} + u_{v0}^2] e^{-\frac{u_{v0}^2}{2\theta_{v0}}}, \\ \int_{v_1 < 0} v_1^4 v_2^2 \frac{1}{2} \frac{\partial_x \theta_{v0}}{\theta_{v0}^2} f_0 dv &= -\frac{1}{2} (\partial_x \theta_{v0}) \frac{\rho_{v0} u_{v0}^3}{\sqrt{2\pi} \theta_{v0}} e^{-\frac{u_{v0}^2}{2\theta_{v0}}} - \frac{5}{2} (\partial_x \theta_{v0}) \frac{\rho_{v0} u_{v0} \theta_{v0}}{\sqrt{2\pi} \theta_{v0}} e^{-\frac{u_{v0}^2}{2\theta_{v0}}} \\ &\quad + (\partial_x \theta_{v0}) \left( \frac{1}{4} \frac{\rho_{v0} u_{v0}^4}{\theta_{v0}} + \frac{3}{2} \rho_{v0} u_{v0}^2 + \frac{3}{4} \rho_{v0} \theta_{v0} \right) \left(1 - \operatorname{erf}\left(\frac{u_{v0}}{\sqrt{2\theta_{v0}}}\right)\right), \\ \int_{v_1 < 0} v_1^2 (v_1 - u)^2 v_2^2 \frac{1}{2} \frac{\partial_x \theta_{v0}}{\theta_{v0}^2} f_0 dv &= -(\partial_x \theta_{v0}) \frac{1}{2} \frac{\rho_{v0} u_{v0} \theta_{v0}}{\sqrt{2\pi} \theta_{v0}} e^{-\frac{u_{v0}^2}{2\theta_{v0}}} \\ &\quad + (\partial_x \theta_{v0}) \rho_{v0} \left( \frac{3}{4} \theta_{v0} + \frac{1}{4} u_{v0}^2 \right) \left(1 - \operatorname{erf}\left(\frac{u_{v0}}{\sqrt{2\theta_{v0}}}\right)\right), \\ \int_{v_1 < 0} v_1^2 v_2^4 \frac{1}{2} \frac{\partial_x \theta_{v0}}{\theta_{v0}^2} f_0 dv &= -(\partial_x \theta_{v0}) \frac{3}{2} \frac{\rho_{v0} u_{v0} \theta_{v0}}{\sqrt{2\pi} \theta_{v0}} e^{-\frac{u_{v0}^2}{2\theta_{v0}}} + (\partial_x \theta_{v0}) \frac{3}{4} \rho_{v0} (u_{v0}^2 + \theta_{v0}) \left(1 - \operatorname{erf}\left(\frac{u_{v0}}{\sqrt{2\theta_{v0}}}\right)\right) \\ \int_{v_1 < 0} v_1^2 v_2^2 v_3^2 \frac{1}{2} \frac{\partial_x \theta_{v0}}{\theta_{v0}^2} f_0 dv &= -(\partial_x \theta_{v0}) \frac{1}{2} \frac{\rho_{v0} \theta_{v0} u_{v0}}{\sqrt{2\pi} \theta_{v0}} e^{-\frac{u_{v0}^2}{2\theta_{v0}}} + (\partial_x \theta_{v0}) \frac{1}{4} \rho_{v0} (u_{v0}^2 + \theta_{v0}) \left(1 - \operatorname{erf}\left(\frac{u_{v0}}{\sqrt{2\theta_{v0}}}\right)\right) \end{aligned} \quad (\text{A31})$$

Recall the expression of energy flux in bulk vapor region (A6), the out-going energy flux is approximated by

$$q_-(x=0) \approx -\frac{2\rho_{v0}\theta_{v0}^2}{\sqrt{2\pi}\theta_{v0}} + \frac{1}{2}q(x=0), \quad (\text{A32})$$

Therefore, by energy conservation we obtain

$$q(x=0) \approx \frac{4\alpha}{2-\alpha} \frac{1}{\sqrt{2\pi}} (\rho_{l0}\theta_{l0}^{3/2} - \rho_{v0}\theta_{v0}^{3/2}). \quad (\text{A33})$$

That is, we can recover the same flux boundary condition for our model as in Chen<sup>55</sup>.

Mass flux and energy flux near the cold liquid, i.e., at  $x=1$ , is approximated by similar computations,

$$\dot{m}(x=1) \approx \frac{2\alpha}{2-\alpha} \left[ \frac{\rho_{v1}\theta_{v1}}{\sqrt{2\pi}\theta_{v1}} - \frac{\rho_{l1}\theta_{l1}}{\sqrt{2\pi}\theta_{l1}} \right], \quad (\text{A34})$$

and

$$q(x=1) \approx \frac{4\alpha}{2-\alpha} \frac{1}{\sqrt{2\pi}} (\rho_{v1}\theta_{v1}^{3/2} - \rho_{l1}\theta_{l1}^{3/2}). \quad (\text{A35})$$

### 3. Semi-continuum solution

The semi-continuum solution is based on the computations in the previous section together with the energy fluxes from liquid films, as in Chen<sup>55</sup>. More specifically, the following nonlinear system is solved for eight unknowns:  $(\dot{m}, q, T_{l0}, T_{l1}, T_{v0}, T_{v1}, \rho_{v0}, \rho_{v1})$ ,

$$\left\{ \begin{array}{ll} \dot{m} = \frac{2\alpha}{2-\alpha} \frac{1}{\sqrt{2\pi}} \sqrt{\frac{k_B}{m_0}} (\rho_{l0}\sqrt{T_{l0}} - \rho_{v0}\sqrt{T_{v0}}), & \text{(vapor mass flux near hot liquid)} \\ \dot{m} = \frac{2\alpha}{2-\alpha} \frac{1}{\sqrt{2\pi}} \sqrt{\frac{k_B}{m_0}} (\rho_{v1}\sqrt{T_{v1}} - \rho_{l1}\sqrt{T_{l1}}), & \text{(vapor mass flux near cold liquid)} \\ q = k_w \frac{T_{w0}-T_{l0}}{d_0} - \dot{m}\Gamma, & \text{(heat flux in hot liquid)} \\ q = k_w \frac{T_{l1}-T_{w1}}{d_1} - \dot{m}\Gamma, & \text{(heat flux in cold liquid)} \\ q = \frac{4\alpha}{2-\alpha} \frac{1}{\sqrt{2\pi}} \left(\frac{k_B}{m_0}\right)^{3/2} (\rho_{l0}T_{l0}^{3/2} - \rho_{v0}T_{v0}^{3/2}), & \text{(vapor energy flux near hot liquid)} \\ q = \frac{4\alpha}{2-\alpha} \frac{1}{\sqrt{2\pi}} \left(\frac{k_B}{m_0}\right)^{3/2} (\rho_{v1}T_{v1}^{3/2} - \rho_{l1}T_{l1}^{3/2}), & \text{(vapor energy flux near cold liquid)} \\ q = c_p \dot{m}T - \kappa \frac{dT}{dx}, & \text{(vapor energy flux in the bulk region)} \\ \rho_{v0}T_{v0} = \rho_{v1}T_{v1}, & \text{(constant pressure in vapor)} \end{array} \right. \quad (\text{A36})$$

It should be noted that the last but one condition is equivalent to solve the transport-diffusion equation (A12) with the vapor temperature  $(T_{v0}, T_{v1})$  near boundary.

Table I: Units of Physical Quantities

Notation	Quantity	Unit
$\tau$	relaxation time	s
$f$	molecular distribution function	$\text{kg}\cdot\text{m}^{-3}$
$\rho$	(dimensional) density	$\text{kg}\cdot\text{m}^{-3}$
$u$	average velocity	$\text{m}\cdot\text{s}^{-1}$
$u_0$	typical velocity	$\text{m}\cdot\text{s}^{-1}$
$\theta$	normalized temperature	$\text{m}^2\cdot\text{s}^{-2}$
$T$	temperature	K
$k_B$	Boltzmann constant	$\text{J}\cdot\text{K}^{-1}$
$m_0$	molecular mass	kg
$R$	ideal gas constant	$\text{J}\cdot\text{kg}^{-1}\cdot\text{K}^{-1}$
$\Gamma$	latent heat	$\text{J}\cdot\text{kg}^{-1}$
$k_w$	heat conductivity (of water)	$\text{W}\cdot\text{m}^{-1}\text{K}^{-1}$
$d_0, d_1$	thickness of liquid film	m
$L$	thickness of vapor gap	m
$\dot{m}$	(dimensional) mass flux	$\text{kg}\cdot\text{s}^{-1}\text{m}^{-2}$
$j_e$	(dimensional) energy flux	$\text{W}\cdot\text{m}^{-2}$

## Appendix B: Units

We present the definition and unit of physical quantities appearing in the main article in Table I.